Microchimica Acta (2021) 188:301
https://doi.org/10.1007/s00604-021-04947-2

ORIGINAL PAPER

# Combination of ultrathin micro-patterned MXene and PEDOT: Poly(styrenesulfonate) enables organic electrochemical transistor for amperometric determination of survivin protein in children osteosarcoma

Ping Xu[1] · Chunwen Lu[2] · Dahui Wang[1] · Dong Fu[1]

Received: 14 April 2021 / Accepted: 15 July 2021


**Abstract**
An ultrathin micro-patterned MXene/PEDOT:PSS-based organic electrochemical transistor biosensor was constructed, which can significantly amplify the amperometric signal and transistor's performance. A novel interdigitated OECTs biosensor has been developed for reliable determination of survivin for the following considerations: (1) The synergistic effect of intercalated MXene and ionic PEDOT:PSS enhanced the mobility and volumetric capacitance of OECTs biosensor. (2) Compared with the best previous literatures, our assay demonstrated enhanced detection limit of survivin down to 10 pg $mL^{-1}$, as well as satisfactory selectivity, reproducibility, and reliability. (3) Comparison of OECTs against commercial ELISA kit yielded favorable linearity ($Y = 1.0015*X + 0.0039$) and correlation coefficient ($R^2 = 0.9717$). Those advantages are expected to pave the way to design of an OECTs biosensor with robustness, non-invasiveness, and miniaturization for the point-of-care applications.

**Keywords** Micro-patterned MXene and PEDOT: Poly(styrenesulfonate) · Survivin protein · Interdigitated organic electrochemical transistor · Biomarker · Osteosarcoma

## Introduction

Osteosarcoma, an aggressive malignant cancer, is the most common primary bone tumor originating from the bones, which affected the health of children, adolescents, and young adults and frequently metastasized to lungs, resulting in poor prognosis [1–3]. Especially, the 5-year survival rate for metastatic osteosarcoma drops to 20% and remains virtually unchanged over the past 30 years [1, 4, 5]. Therefore, the early diagnosis of strategies for osteosarcoma patients is necessary and urgent [2, 4–6].

Survivin, 16.5-kD protein, belonging to the inhibitor of apoptosis (IAP) family is an important oncogenic protein expressed highly in osteosarcoma [7–10]. Normal cells did not require survivin for survival; however, survivin is significant for osteosarcoma tumor cells in cell division and inhibition of apoptosis [7, 11]. Besides the functionality of regulation of cell division and inhibition of apoptosis, the elevated level of survivin protein has been regarded as a new potential diagnostic biomarker for osteosarcoma and be used as a reference index to determine pathology classification of osteosarcoma [7, 8, 12].

In the past few years, a lot of techniques, such as the enzyme-linked immunosorbent assay (ELISA) [13], piezometric biosensor [14], and plasmon-enhanced resonance energy transfer [15] have been investigated for the determination of survivin protein. However, these methods have several drawbacks, such as the requirements of expensive clinical equipment, sophisticated procedures, and low sensitivity and selectivity. Therefore, a simple, inexpensive platform for ultrasensitive determination of survivin protein is imperative.

Ping Xu and Chunwen Lu contributed equally to this work.

✉ Dahui Wang
wangdahui@fudan.edu.cn

✉ Dong Fu
fudong@fudan.edu.cn

[1] Department of Orthopedics, Children's Hospital of Fudan University, National Children's Medical Center, Shanghai, China

[2] Department of Orthopedics, Changhai Hospital, Second Military Medical University, Shanghai, China

Published online: 18 August 2021

Organic electrochemical transistors (OECTs) have demonstrated huge potential and advantages for biological and biochemical sensing applications due to their unique merits, such as high sensitivity, low operation voltage, biocompatibility and flexibility, and simplified fabrication processes, which allow them to be operated in the aqueous environment [16–18]. The OECTs biosensors based poly(3,4-ethylenedioxythiophene) poly(styrenesulfonate) (PEDOT/PSS) have been widely applied for sensing of bacteria [19], dopamine [20], DNA [21], cells [22], and ions [23], and above-mentioned examples displayed that the sensitivity of OECTs is superior to those conventional methodology [24–26].

Ti3C2Tx is one typical member of the growing club of 2D layered early-transition metal carbides/carbonitrides (MXenes) ($T_x$ denotes surface-terminating functionality (e.g., F, O, and OH)) [27–29], which displays great promise for biosensor design and fabrication, including following advantages: (1) high excellent metallic conductivity up to 9880 S $cm^{-1}$; (2) high capacitance up to 1500 F $cm^{-3}$, originating from the intercalation/deintercalation of $H^+$ and redox interreaction; and (3) the hydrophilic surface of Ti3C2Tx MXene makes it suitable for various solution processing, such as spray coating and spinning coating for making biosensor devices in aqueous environment [27, 30, 31]. Compared with nanomaterials such as PPy, PANI, rGO, C-dots, AuNPs, and ZnO, unique intercalation/deintercalation nanostructures enable MXene@PEDOT: PSS as an ideal binder candidate to achieve the high-performance OECTs biosensor with high volumetric capacitance in a synergistic manner [27, 30].

In this paper, we proposed label-free, highly sensitive, and selective organic electrochemical transistor biosensor to detect the survivin protein via combination of ultrathin micropatterned MXene and PEDOT: PSS. Moreover, our assay afforded the enhanced detection limit of survivin protein down to 10 pg $mL^{-1}$ (S/N>3), as well as satisfactory selectivity, reproducibility, and reliability, superior to the best previous literatures. Finally, the clinical performance of the OECTs biosensor were evaluated against commercial technique (ELISA).

## Experiment

### Materials

Recombinant human survivin protein (ab87202), Anti-Survivin (ab76424), cluster of differentiation 44 (CD44), cluster of differentiation 63 (CD63), and prostate specific antigen (PSA) was purchased from Abcam, Inc. (https://www.abcam.cn, Cambridge, MA). The commercial survivin protein kit was provided by Jianglai Biological Co., Ltd. (http://jianglai.foodmate.net, detection range of 8–640 pg $mL^{-1}$). MAX phase $Ti_3AlC_2$ is provided by Xian Ruixi Biotechnology Co. (https://ruixibio.company.lookchem.cn, China). Hydrochloric acid (HCl), mercaptoacetic acid (MAA, CAS: 68-11-1), and lithium fluoride (LiF) with analytical purity were bought from Sinopharm Chemical Reagent Co., Ltd. (https://www.sinoreagent.com, Shanghai, China). 6-Mercapto-1-hexanol (MCH), ethylene glycol, BSA (bovine serum albumin), glucose, lysine, tyrosine, and (3-glycidyloxypropyl) trimethoxysilane (GOPS) were purchased from Sigma Chemical Co. (http://www.sigmaaldrich.com, St. Louis, MO). The dimethyl sulfoxide (DMSO), potassium ferricyanide ($K_3[Fe(CN)_6]$), and potassium ferrocyanide ($K_4[Fe(CN)_6]$) were purchased from Aladdin Chemicals Co., Ltd. (https://www.aladdin-e.com). The PEDOT: PSS (PH 1000, CAS: 155090-83-8) aqueous solutions was purchased from Heraeus Clevios GmbH (https://www.heraeus.cn/cn/group/home/home.html, Germany, Leverkusen). Ultrapure deionized (DI) water was obtained by a Milli-Q system (https://www.emdmillipore.com/US/en, MΩ•cm @ 25 °C: 18.2 M, Millipore, Bedford, MA, USA). Phosphate buffered saline and all other chemicals, unless mentioned, were purchased from Sigma-Aldrich.

### Fabrication of MXene and preparation of MXene@PEDOT: PSS

$Ti_3C_2$ was successfully prepared by etching Al from $Ti_3AlC_2$ in HF according to previous literatures [32, 33]. $Ti_3C_2$ was synthesized by selectively etching the Al layer from $Ti_3AlC_2$ in LiF/HCl aqueous solution. Briefly, 0.99 g of LiF was dissolved in 20 mL of HCl under magnetic stirring for 15 min, and then 1.25 g of $Ti_3AlC_2$ was added slowly (10 min) to the HCL solution. The mixture was further stirred for 10 h at 40 °C. Then, the resulting MXene suspension was repeatedly washed 6 times using deionized water until the pH value reached ~6.4. Finally, the powder was dried in the vacuum oven at 45 °C for 12 h, and the final product was freeze-dried for 12 h.

Before preparation of MXene@PEDOT: PSS, the PEDOT: PSS (Clevios PH 1000) was firstly doped with DMSO (5% by volume), GOPS surfactant (0.025% by volume), and ethylene glycol (10% by volume) and filtered via organic microporous membrane (Millipore 0.22 μm, 47 mm, Nylon). Then, the MXene@PEDOT: PSS composites were prepared by dropwise addition of a mixture of PEDOT: PSS into the colloidal solution of MXene. The mixture was filtered via nanoporous polypropylene membranes (0.06 μm pore size) in air.

### Fabrication of OECTs device

The native oxide $p^+$ silicon substrates (size: 1.5 × 1 cm) were first rinsed with acetone, isopropanol, and water and then

properly dried. The p+ silicon substrate was patterned by photoresist S1813 (Shipley) and customized shadow mask for proposed architecture in Fig. S2a. The patterned Cr/Au source and drain electrodes (thicknesses: 5 nm/45 nm) were deposited on substrates by thermal evaporation deposition under different channel architectures (Fig. S2). The working pressure and thickness for thermal evaporation deposition were 1.2 Pa and 10 nm for Cr deposition (acting as an adhesion layer) and 0.5 Pa and 50 nm for Au deposition, respectively. Consequently, a layer of active semiconducting material was deposited in the channel, and the wafer was washed with deionized water, blow dried with nitrogen gun, and baked for 30 s at 120°C.

### Apparatus

Characterizations of materials and sensors include scanning electron microscopy (SEM), transmission electron microscopy (TEM), contact angle, atomic force microscopy (AFM), electrochemical impedance spectroscopy (EIS), and differential pulse voltammetry (DPV). The SEM characterization was performed by Hitachi S-4800 (https://www.hitachi.com/) at an accelerating voltage 10 kV with 160000× magnifications. The contact angle was carried by Data Physics SZ-CAMA1 drop measurement (https://www.dataphysics-instruments.com/), where 10 μL of purified water droped on the gate electrodes for characterization. The AFM was conducted by Dimension Icon & FastScan Bio (https://www.bruker.com/de.html, Bruker Nano, CA, USA) in the resonance frequency range of 90–350 kHz under tapping mode. The transistor characteristics of biosensor were performed by Keithley 2635B (https://www.tek.com/keithley, Tektronix Co.). The biosamples were centrifuged by TGL-16G centrifuge (http://www.antinglxj.com/cp/gslxj/tgl-16g.html, Shanghai Anting Science Instrument, Shanghai).

The electrochemical properties of sensors were characterized via the electrochemical station (http://www.chinstr.com/, CHI650D, Shanghai, Chenghua). For the DPV electrochemical characterization, the voltage was scanned from 0 to 500 mV with a pulse amplitude of 15 mV, a scan rate of 10 mV/s, a pulse width of 50 ms, and a quiet time of 4 s. For the EIS characterization, the frequency was conducted from 10000 to 0.05 Hz with a pulse amplitude of 5 mV.

### Configurations and calibration for OECTs

The source, drain, and gate electrodes of the OECTs were linked to two-channel sourcemeter instrument (Keithley 2635B, https://www.tek.com/keithley, Tektronix Co.). A customizable program was designed to modulate gate voltages ($V_G$) and source-drain voltages ($V_{DS}$). As displayed in Fig. S2, the OECTs biosensor assembled with interdigitated source and drain electrodes, and anti-survivin modified gate electrode was immersed into the PBS ionic liquid electrolyte.

The binding between the various amounts of survivin protein and anti-survivin modified gate electrode can modulate $I_{DS}$ under the fixed operational $V_G$. To characterize the responses of the OECTs-based biosensor for various concentrations of survivin protein, the sensor was measured at fixed gate and drain voltages: $V_G$=0.85, $V_{DS}$=0.08. In the determination of time-dependent channel currents ($I_{DS}$ versus time). For the configuration of transfer characteristics, $I_{DS}$ was tested at a fixed source-drain voltage ($V_{DS}$ = 0.08 V) at various gate voltages ($V_G$: 0~1.1 V) with a sweeping rate of 0.02 $Vs^{-1}$. For the configuration of output characteristics ($I_{DS}$ vs $V_D$), the $V_G$ was fixed at 0.9 V at various drain voltages ($V_D$: 0–0.2 V) with a scanning rate of 0.01 V/s.

For the calibration plot of survivin protein on OECTs, the survivin antibody (anti-survivin, 10 μg/mL) functionalized gate electrode of the OECTs device was incubated in survivin protein solution for 0.5 h, followed by three times washing with PBS. The detection limit of each device was defined by the channel current response at a signal/noise ratio of 3.

### Harvesting of clinical biosamples

All clinical research and protocols in this project were authorized by the institutional ethics committee of the Children's Hospital of Fudan University (Reference No: 202153). For the protocols of biosample collection, 10 mL of biosamples was centrifuged at 1000 ×g for 5 min, and the resulting supernatant was obtained in EDTA anticoagulant tube (purple tube) and stored at −20 °C for further detection.

### Statistical analysis

All statistical analysis in this work such as calibration plot, standard deviation (S.D.), *t*-test, and relative standard deviation (RSD) were calculated by the SPSS software (version 16.0, SPSS Statistics, Inc., Chicago, USA).

## Results and discussion

### Preparation of MXene@PEDOT: PSS nanocomposites

The procedures for preparation of the MXene@PEDOT: PSS nanocomposites film and fabrication of the OECTs semiconducting membrane were schematically illustrated in Fig. 1 (see details in the "Experiment" section). For the synthesis of MXene, $Ti_3C_2$ was synthesized by selectively etching the Al layer from $Ti_3AlC_2$ in LiF/HCl aqueous solution. As displayed in Fig. S1, the micro-patterned MXene created abundant active site for biosensing. As shown in Fig. 1a, the MXene/PEDOT: PSS nanocomposites were structurally

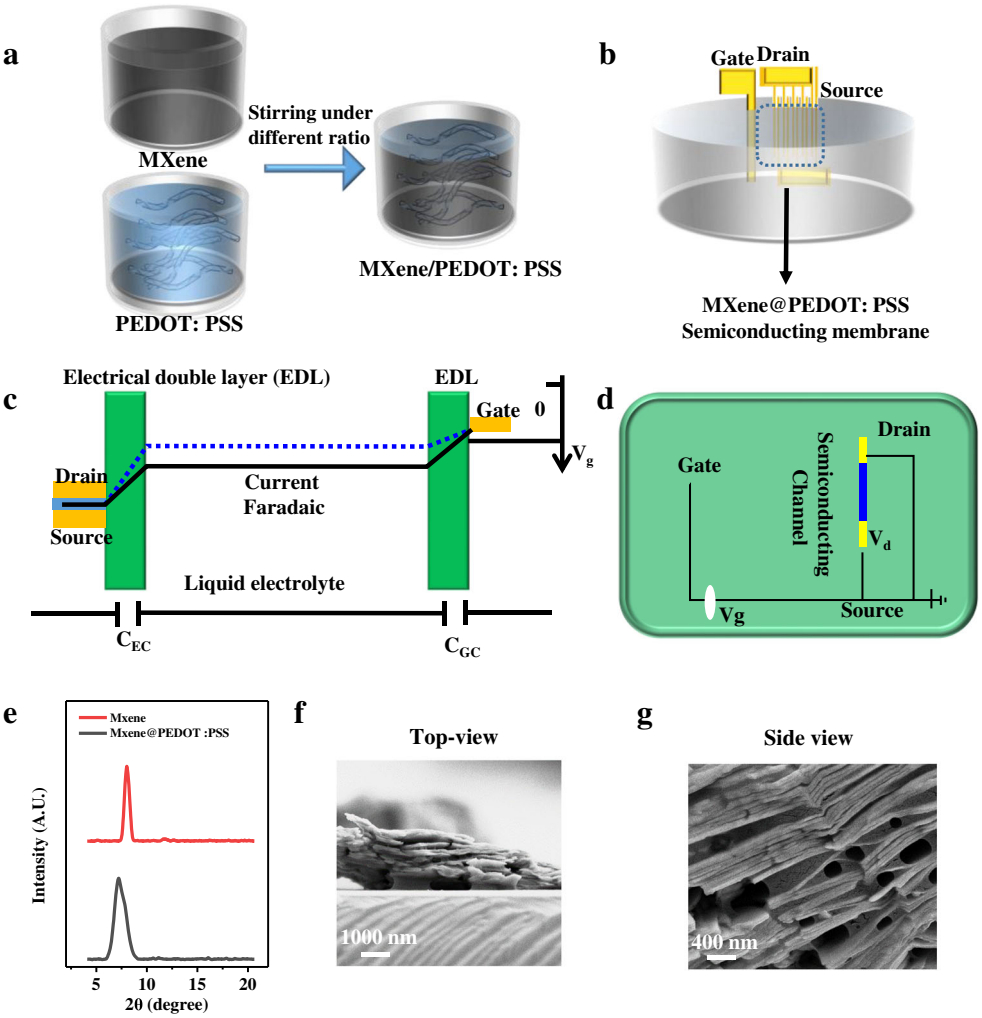


**Fig. 1** Schematic representation for OECTs survivin biosensor. **a** The preparation of MXene@PEDOT: PSS nanocomposites. **b** Schematic illustration of OECTs biosensor for the sensing of survivin protein. **c** OECTs biosensor with modified gate electrode characterized in the liquid electrolyte via the double electronic layer capacitance in the **d** equivalent circuit. **e** XRD analysis of pure MXene and MXene@PEDOT: PSS nanocomposites. **f** Top view and **g** side view characterization of MXene@PEDOT: PSS by SEM. $C_{GE}$ is the capacitance of gate/electrolyte interface, and the $C_{EC}$ is the capacitance of electrolyte/channel interface.

rearranged under stirring. For the characterization, the X-ray diffraction (XRD) was selected to analyze the chemical composition of the fabricated MXene and rearranged MXene@PEDOT: PSS, demonstrating the transformation of MXene to MXene@PEDOT: PSS (Fig. 1e) [27]. The micro-patterned structure of MXene@PEDOT: PSS was also characterized by SEM images including the side view (Fig. 1f) and top view (Fig. 1g). Compared with the pure PEDOT: PSS, the micro-patterned MXene@PEDOT: PSS revealed the combination and rearrangement of MXene and PEDOT: PSS.

## Fabrication and optimization of OECTs

We designed the OECTs biosensor for survivin protein detection (Fig. 1) via micro-patterned MXene@PEDOT: PSS as the semiconducting materials. The OECTs biosensor includes three components, which were depicted as follows: the gate, the interdigitated drain-source electrode, and the MXene@PEDOT: PSS semiconducting films as illustrated in Fig. 1b and c. The OECTs biosensor with modified gate electrode was measured in the liquid electrolyte via the double electronic layer capacitance in the equivalent circuit. Afterwards, source-drain electrodes with interdigitated architecture and functionalized gate electrode were immersed into the PBS liquid electrolyte for characterization and quantitative analysis (Fig. 1a). The higher Faradaic current can be induced by higher concentration of survivin protein. Accumulated survivin molecules in the vicinity of the gate electrode would modulate $I_{DS}$ of the channel. The binding of survivin to the gate electrode reduces the $I_{DS}$ of OECTs biosensor due to the volumetric capacitance effect.

Notably, a specific anti-survivin modification was used to capture survivin protein in Fig. 2a and Fig. S2b, and the gate electrode was immersed in the solution of mercaptoacetic acid (MAA) for carboxylation. To certify the functionalization process of the gate electrode, we characterized CV, EIS, and contact angle and AFM. Firstly, we conducted EIS (Fig. 2b) for certification of layer-by-layer processes. The EIS displayed $R_{et}$ of 347.5 Ω (black curve in Fig. 2b) for original status. Subsequently, the EIS values for Au/MAA/anti-survivin (red curve in Fig. 2b) and Au/MAA/anti-survivin/BSA (green curve in Fig. 2b) were measured up to 359.2 Ω

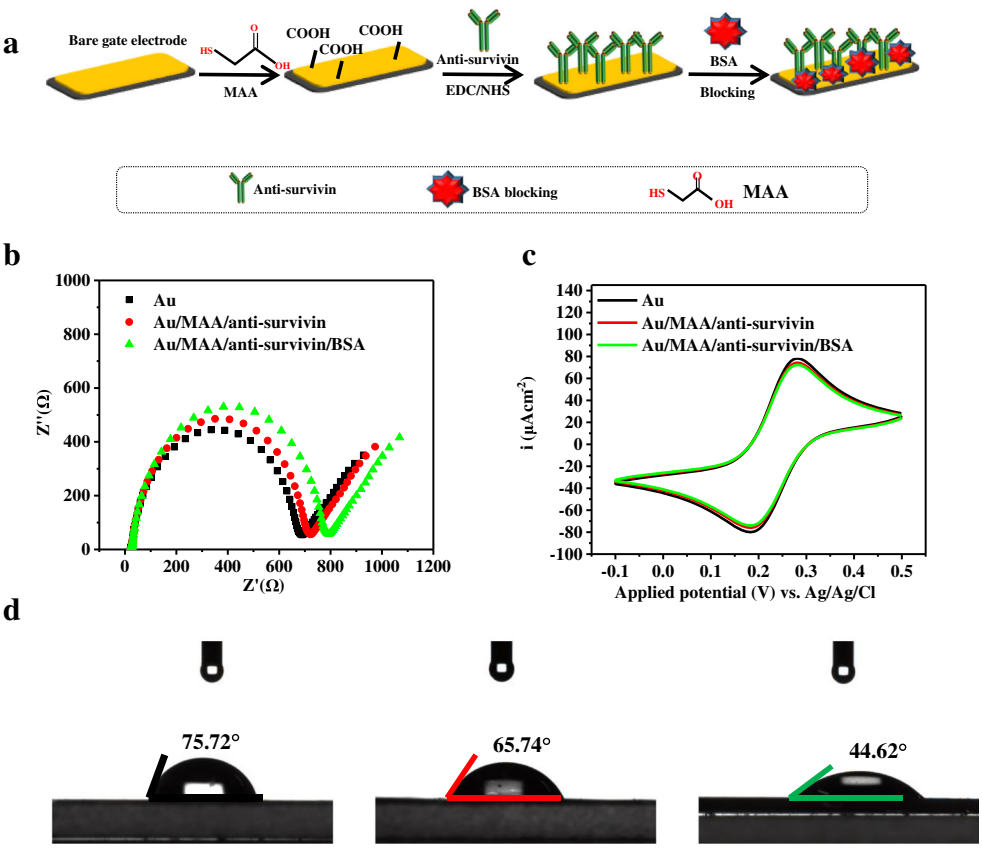


**Fig. 2** Depiction of layer-by-layer assembly on gate electrode. **a** Procedures for functionalization of gate electrode. **b** EIS, **c** cyclic voltammetry, and **d** contact angle analysis of bare Au, Au/MAA/anti-survivin, and Au/MAA/anti-survivin/BSA, respectively.

and 385.2 Ω, respectively. For CV analysis (Fig. 2c), the bare Au electrode displayed redox current of 78.2 μA at 293 mV (vs. Ag/AgCl). For comparison, after modification, the response current declined to 74.3 μA and 72.3 μA for the Au/MAA/anti-survivin and Au/MAA/anti-survivin/BSA, respectively. Meanwhile, in the scan rate dependence study (Fig. S3) in a mixture solution of 10 mM $K_3[Fe(CN)_6]/K_4[Fe(CN)_6]$, the electrochemical current and the square root of scan rate ($V^{1/2}$) displayed a linear characteristic, indicating a surface-controlled processes with a linear relationship of $i_{redox} = 8.28 \times V^{1/2} - 23.57$ (correlation coefficient of 0.9985, Fig. S3). The phenomenon suggested the excellent properties of the gate electrode in the process of electron efficient transportation.

For the hydrophobicity/hydrophilicity analysis, the contact angle for bare Au electrode was 75.72° (Fig. 2d), and the values decreased to 65.74° and 44.62°, respectively, after the modification of anti-survivin and the BSA. AFM was conducted to investigate the morphological change of the sensor (Fig. S4). The root mean square (rms) roughness would reflect the morphology features of sensors including bare Au (5.6 ± 1.1 nm), Au/MAA (58.7 ± 9.4 nm), Au/MAA/anti-survivin (89.2 ± 11.3 nm), and Au/MAA/anti-survivin/BSA (121.5 ± 8.5 nm), demonstrating the layer-by-layer modification process on the bare Au electrode. Collectively, above-mentioned CV, EIS, contact angle, and AFM characterizations demonstrated the successful functionalization of gate electrode for determination of survivin protein.

Tunable architecture of OECTs enhances the transconductance, and the transconductance can also be calculated by the following equation:

$$G_m = \frac{Wd}{L}\mu C^*(V_{th} - V_G) \quad (1)$$

where $C^*$ is the volumetric capacitance and $V_{th}$ is the threshold voltage. The volumetric capacitance reflects the capabilities of carrier/ionic transport and the efficiency of ion-to-electron efficiency. Details for mechanism of OECTs were illustrated in the Supporting Information. The performances of MXene@PEDOT: PSS in different ration were demonstrated in Fig. S5. And the optimized transconductance reached 0.992 mS, indicating high sensitivity of OECTs device for determination of survivin protein. EIS were performed to study the volumetric capacitance. An equivalent circuit model of impedance was selected: $R_s$ (CPE||$R_{ct}$), where $R_s$ is the resistance of the liquid electrolyte and $R_{ct}$ represents the resistance of the micro-patterned MXene@PEDOT: PSS membrane (Fig. S6a) [34, 35]. The CPE represented constant phase element, which was widely used to represent the electrochemical properties of OECTs. The volumetric capacitance $C^*$ can be extracted from the equivalent circuit model.

As displayed in Fig. S6 and Table S1, the volumetric capacitance was calculated with the value of 74.1±8.6 F/cm$^3$, representing favorably comparable parameters against OECTs nanocomposites.

## Sensing performance of OECTs for survivin protein

Parameter optimization including the pH, incubation time, temperature, and the concentration of surviving antibody was performed to optimize the significant factor, which was illustrated in Fig. S7 to improve the sensing performance. The optimized parameters were fixed as follows: pH=7.0, incubation time of 30 min, temperature=37 °C, and concentration of antibody-$_{survivin}$ of 10 μg/mL. Fig. 3a demonstrated the channel current responses of the OECTs device to addition of various concentration survivin protein. The higher concentration of protein solution used for capture of gate electrode, the lower channel current change ($I_{DS}$) was observed, indicative of the monotonic relationship between the concentration of targeted survivin protein and the variation of channel current change. In Fig. 3b, the signal-to-noise ratio (S/N) >3 satisfied the requirements of detection limit ($10^{-2}$ ng mL$^{-1}$) [36, 37]. On the contrary, the channel current slightly changed without the functionalization of anti-survivin (Fig. S8), illuminating the working mechanism

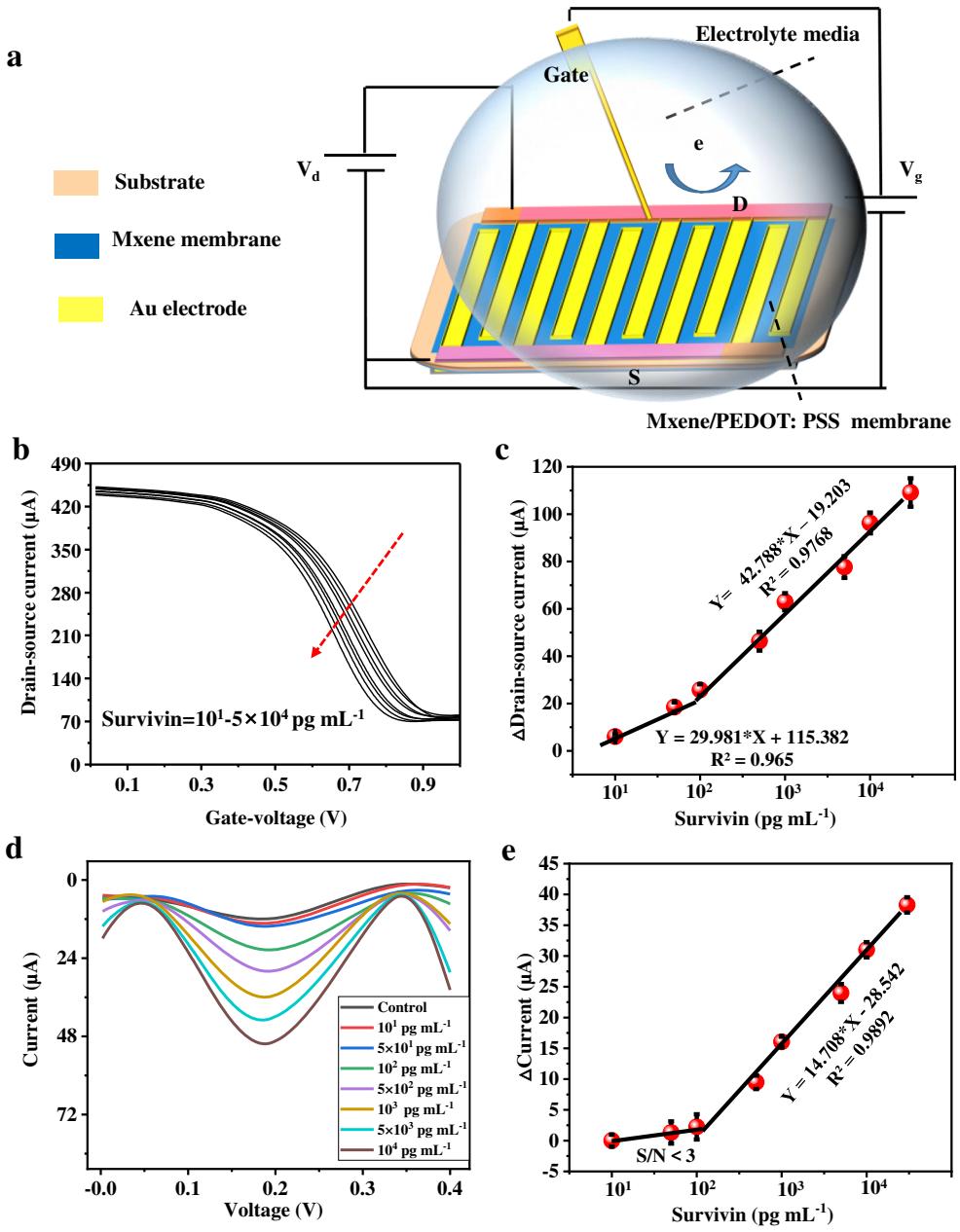


**Fig. 3** Depiction of detection mechanism. **a** Proposed mechanism of OECT via the combination of ultrathin micro-patterned MXene and PEDOT:PSS. **b** The transfer characteristics measurement ($I_{DS}$-t) responses of the devices to the addition of survivin protein. **c** Change in drain-source current as a function of survivin protein concentration. **d** Conventional differential pulse voltammetry analysis of the Au gates as the work electrode in the incubation of survivin protein. **e** Calibration plot of the DPV determination as a function of survivin protein concentration. Each of the error bars in panels **c** and **e** represents the three replicate determinations ($n$ = 3, standard deviation).

of OECTs. As shown in Fig. 3c, the proposed OECTs achieved sensitive quantification of survivin with ultra-wide linear range $10^1$–$10^2$ and $10^2$–$5\times10^5$ ng mL$^{-1}$, and the linear corresponding regression curve was $\triangle I_{DS}$ (μA) = 29.98× log [concentration$_{survivin}$] + 115.38 ($R^2$ = 0.96) and $\triangle I_{DS}$ (μA) = 42.78× log [concentration$_{survivin}$] − 19.20 ($R^2$ = 0.97, respectively. In comparison, the anti-survivin-modified gated electrode was also performed as the working electrode in conventional differential pulse voltammetry (DPV) assay (Fig. 3d). The limit of detection (LOD) was 100 pg mL$^{-1}$ (S/N = 3) with the sensitivity of 35.3 μA (ng mL$^{-1}$)$^{-1}$ cm$^{-2}$ (Supporting Information, S8). The sensitivity was estimated by the slope values, which derived from linear plots of oxidation peak currents [38, 39]. However, the performance in the low concentration range could not meet requirement of S/N ratio, indicating high sensitivity of our sensor for the quantification of survivin protein. Comparisons of survivin performance with other biosensors were summarized in Table S2, manifesting comparable performance with the majority of other type of biosensors (ELISA, magnetic beads, fluorescent type), due to the ultrathin micropatterned MXene@PEDOT: PSS.

## Selectivity, reproducibility, and reliability

To evaluate the selectivity of OECTs for survivin determination, the $I_{DS}$ VS t measurement was performed by adding interfering molecules. We selected typical high-molecular weight proteins (CD63, PSA CD44) and low-molecular weight molecules (glucose, tyrosine, lysine) as interferences. As depicted in Fig. 4a–b, $I_{DS}$-t curves demonstrated high response of △current in sensing of 1 ng mL$^{-1}$ survivin (14.01 ± 0.4 μA). For comparisons, we recorded low responses in detecting of 10 ng mL$^{-1}$ CD44 (0.31 ± 0.31), PSA (0.33 ± 0.27), CD63 (0.33 ± 0.27), glucose (0.42 ± 0.03), lysine (0.33 ± 0.27), and tyrosine (0.45 ± 0.29). Meanwhile, we tested the △current responses of five sensors in determination of 1 ng mL$^{-1}$ survivin to evaluate the reproducibility. The RSD of 2.33% (Fig. 4c) demonstrated high reproducibility of OECTs sensor. For monitoring of stability (Fig. 4d). Compared with original response (445 ± 8.2 μA), after monitoring of 1 week (443.3 ± 8.12 μA), 2 weeks (440.1 ± 8.24 μA), 1 month (438.1 ± 8.14 μA), and 2 months (436.5 ± 8.22 μA), the $I_{DS}$ displayed negligible change with decline of $I_{DS}$ by < 4%.

Recovery test was performed via adding the different concentration of survivin into PBS (Table S3) to evaluate the practical applications of our sensor. Satisfactory recovery rate kept within 96.9–103.7% with maximum RSD of 11.09%. Those above-mentioned results manifested satisfactory selectivity, reproducibility, and stability of our OECTs sensor for the determination of survivin protein.

## Clinical applications for osteosarcoma biosamples

For clinics, this novel OECTs were utilized for survivin sensing in serum clinical biosamples. A series of patient's serum samples were collected via standard protocol ("Experiment" section), and the survivin values were tested by commercial ELISA kit with calibration plot in Fig 5a. The differentiation

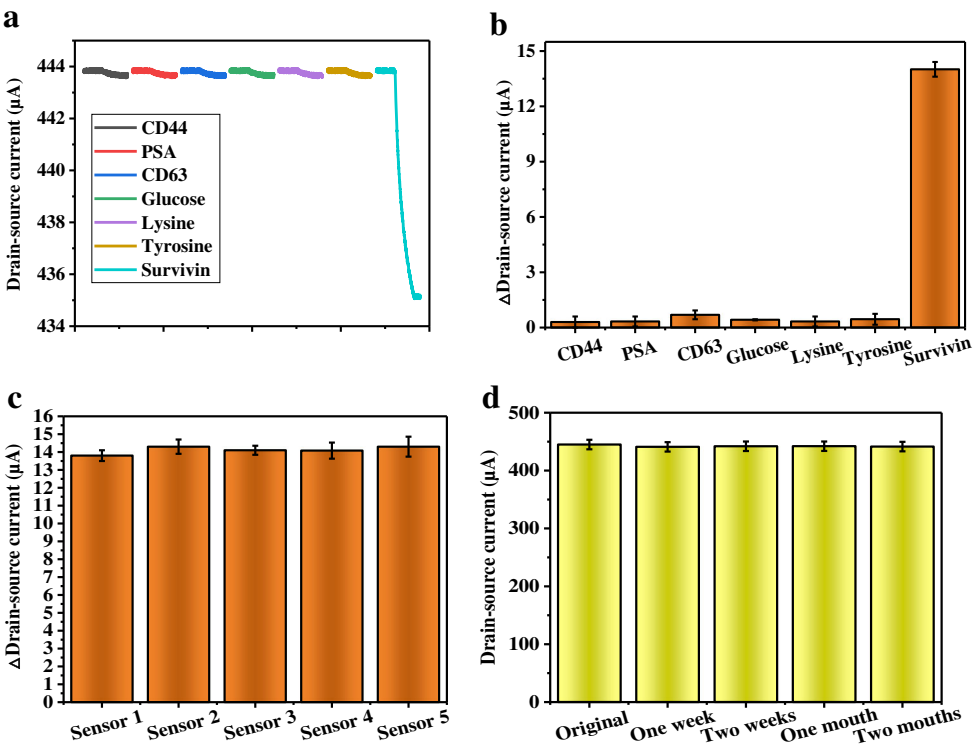


**Fig. 4** Performance assessments. a–b Selectivity test: i-t curve of OECTs device responses to survivin protein and other interferences, **c** repeatability, and **d** stability of OECT device response to 100 pg mL$^{-1}$ survivin.

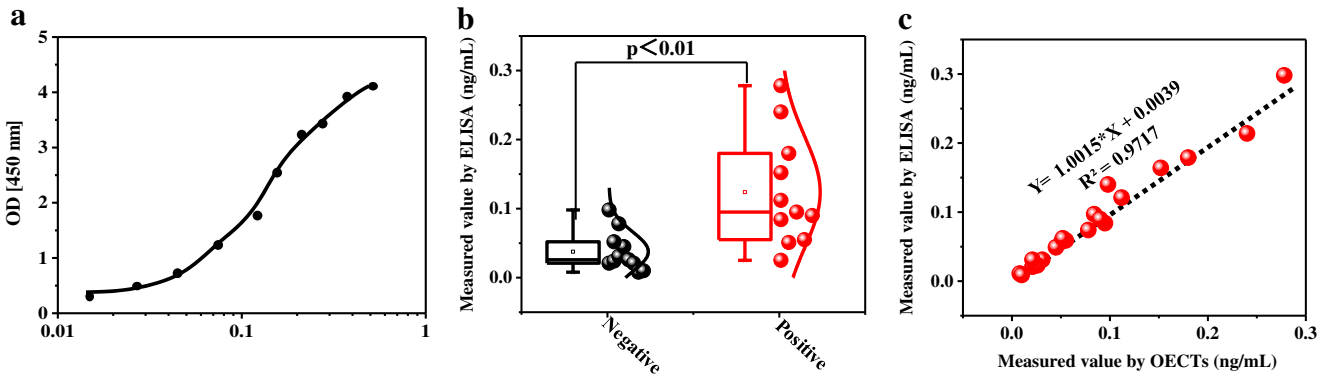


**Fig. 5** Clinical evaluations. **a** Calibration plot of commercial ELISA kit for survivin protein, **b** differentiation of OECT for 22 clinical biosamples, and **c** corresponding correlation.

of positive and negative sample was illustrated in Fig.5b ($N_{positive}$=11, $N_{negative}$=11, $p$<0.01, Table S4). Moreover, as shown in Fig. 5c, linear correlation of serum survivin concentration was performed between the measured values and ELISA values with the linear correlation curve ($Y$ = 1.0015*$X$ + 0.0039, $R^2$ = 0.9717), advocating comparable clinical performance of OECTs against commercial ELISA kit.

## Conclusions

In this work, a nanocomposite was prepared by combination of micro-patterned MXene and PEDOT: PSS. Following that, a conceptually OECTs survivin biosensor was fabricated via MXene@PEDOT: PSS nanocomposite and antibody functionalization for highly sensitive determination of survivin protein, and the OECTs biosensor including corresponding surface morphology, structure, composition, and electrical properties was then characterized by SEM, XRD, and contact angle, AFM, cyclic voltammetry, EIS, and sourcemeter. The biosensor demonstrated ultrasensitivity of survivin down to the level of 10 pg $mL^{-1}$ as well as acceptable reliability, selectivity, reproducibility, and practical applications of complex biosamples with satisfactory linear correlation against commercial ELISA kit. Considering the above-mentioned merits, we anticipate that micro-patterned MXene@PEDOT: PSS paves a convenient and versatile platform for organic semiconductor biosensors in the detection of cancer-relevant biomarkers.

**Author contribution** Ping Xu: Conceptualization, methodology, investigation, writing-original draft, and formal analysis. Chunwen Lu: Investigation, writing-original draft, and software. Dahui Wanga: Writing-original draft. Dong Fu: Methodology, supervision, and writing-review and editing.

**Funding** The research leading to these results received funding from Shanghai Key Laboratory of Pediatric Gastroenterology and Nutrition (17DZ2272000).

## Declarations

**Conflict of interest** The authors declare no competing interests.

## References

1. Isakoff MS, Bielack SS, Meltzer P, Gorlick R (2015) Osteosarcoma: current treatment and a collaborative pathway to success. J Clin Oncol Off J Am Soc Clin Oncol 33:3029–3035. https://doi.org/10.1200/JCO.2014.59.4895
2. Sayles LC, Breese MR, Koehne AL, Leung SG, Lee AG, Liu H-Y, Spillinger A, Shah AT, Tanasa B, Straessler K, Hazard FK, Spunt SL, Marina N, Kim GE, Cho S-J, Avedian RS, Mohler DG, Kim M-O, DuBois SG, Hawkins DS, Sweet-Cordero EA (2019) Genome-informed targeted therapy for osteosarcoma. Cancer Discov 9:46–63. https://doi.org/10.1158/2159-8290.CD-17-1152
3. Janus AM, Faryna M, Haberko K, Rakowska A, Panz T (2008) Chemical and microstructural characterization of natural hydroxyapatite derived from pig bones. Microchim Acta 161:349–353. https://doi.org/10.1007/s00604-007-0864-2
4. Wang X, Qin G, Liang X, Wang W, Wang Z, Liao D, Zhong L, Zhang R, Zeng Y-X, Wu Y, Kang T (2020) Targeting the CK1α/CBX4 axis for metastasis in osteosarcoma. Nat Commun 11:1141. https://doi.org/10.1038/s41467-020-14870-4
5. Kansara M, Teng MW, Smyth MJ, Thomas DM (2014) Translational biology of osteosarcoma. Nat Rev Cancer 14:722–735. https://doi.org/10.1038/nrc3838
6. Gianferante DM, Mirabello L, Savage SA (2017) Germline and somatic genetics of osteosarcoma - connecting aetiology, biology and therapy. Nat Rev Endocrinol 13:480–491. https://doi.org/10.1038/nrendo.2017.16
7. Shoeneman JK, Ehrhar EJ 3rd, Eickhoff JC, Charles JB, Powers BE, Thamm DH (2012) Expression and function of survivin in canine osteosarcoma. Cancer Res 72:249–259. https://doi.org/10.1158/0008-5472.CAN-11-2315
8. Gu J, Ji Z, Li D, Dong Q (2019) Proliferation inhibition and apoptosis promotion by dual silencing of VEGF and Survivin in human

osteosarcoma. Acta Biochim Biophys Sin Shanghai 51:59–67. https://doi.org/10.1093/abbs/gmy146
9. Mariani F, Quast T, Andronescu C, Gualandi I, Fraboni B, Tonelli D, Scavetta E, Schuhmann W (2020) Needle-type organic electrochemical transistor for spatially resolved detection of dopamine. Microchim Acta 187:1–11. https://doi.org/10.1007/s00604-020-04352-1
10. Peng J, He T, Sun Y, Liu Y, Cao Q, Wang Q, Tang H (2018) An organic electrochemical transistor for determination of microRNA21 using gold nanoparticles and a capture DNA probe. Microchim Acta 185:2–10. https://doi.org/10.1007/s00604-018-2944-x
11. Yang D, Welm A, Bishop JM (2004) Cell division and cell survival in the absence of survivin. Proc Natl Acad Sci U S A 101:15100–15105. https://doi.org/10.1073/pnas.0406665101
12. Liu Y, Teng Z, Wang Y, Gao P, Chen J (2015) Prognostic significance of survivin expression in osteosarcoma patients: a meta-analysis. Med Sci Monit Int Med J Exp Clin Res 21:2877
13. Khan S, Aspe JR, Asumen MG, Almaguel F, Odumosu O, Acevedo-Martinez S, De Leon M, Langridge WHR, Wall NR (2009) Extracellular, cell-permeable survivin inhibits apoptosis while promoting proliferative and metastatic potential. Br J Cancer 100:1073–1086. https://doi.org/10.1038/sj.bjc.6604978
14. Stobiecka M, Chalupa A, Dworakowska B (2016) Piezometric biosensors for anti-apoptotic protein survivin based on buried positive-potential barrier and immobilized monoclonal antibodies. Biosens Bioelectron 84:37–43. https://doi.org/10.1016/j.bios.2015.10.041
15. Stobiecka M, Chalupa A (2015) Modulation of plasmon-enhanced resonance energy transfer to gold nanoparticles by protein survivin channeled-shell gating. J Phys Chem B 119:13227–13235. https://doi.org/10.1021/acs.jpcb.5b07778
16. Sun H, Vagin M, Wang S, Crispin X, Forchheimer R, Berggren M, Fabiano S (2018) Complementary logic circuits based on high-performance N-type organic electrochemical transistors. Adv Mater 30:1–7. https://doi.org/10.1002/adma.201704916
17. Savagian LR, Österholm AM, Ponder JF, Barth KJ, Rivnay J, Reynolds JR (2018) Balancing charge storage and mobility in an oligo(ether) functionalized dioxythiophene copolymer for organic- and aqueous-based electrochemical devices and transistors. Adv Mater 30:1–6. https://doi.org/10.1002/adma.201804647
18. Fu Y, Wang N, Yang A, Law HK w, Li L, Yan F (2017) Highly sensitive detection of protein biomarkers with organic electrochemical transistors. Adv Mater 29:1–7. https://doi.org/10.1002/adma.201703787
19. Méhes G, Roy A, Strakosas X, Berggren M, Stavrinidou E, Simon DT (2020) Organic microbial electrochemical transistor monitoring extracellular electron transfer. Adv Sci 7:2000641. https://doi.org/10.1002/advs.202000641
20. Xie K, Wang N, Lin X, Wang Z, Zhao X, Fang P, Yue H, Kim J, Luo J, Cui S, Yan F, Shi P (2020) Organic electrochemical transistor arrays for real-time mapping of evoked neurotransmitter release in vivo. Elife 9. https://doi.org/10.7554/eLife.50345
21. Song J, Lin P, Ruan Y-F, Zhao W-W, Wei W, Hu J, Ke S, Zeng X, Xu J-J, Chen H-Y, Ren W, Yan F (2018) Organic photoelectrochemical transistor-based biosensor: a proof-of-concept study toward highly sensitive DNA detection. Adv Healthc Mater 7:e1800536. https://doi.org/10.1002/adhm.201800536
22. Guo X, Cao Q, Liu Y, He T, Liu J, Huang S, Tang H, Ma M (2020) Organic electrochemical transistor for in situ detection of H(2)O(2) released from adherent cells and its application in evaluating the in vitro cytotoxicity of nanomaterial. Anal Chem 92:908–915. https://doi.org/10.1021/acs.analchem.9b03718
23. Keene ST, Fogarty D, Cooke R, Casadevall CD, Salleo A, Parlak O (2019) Wearable organic electrochemical transistor patch for multiplexed sensing of calcium and ammonium ions from human perspiration. Adv Healthc Mater 8:e1901321. https://doi.org/10.1002/adhm.201901321
24. Ohayon D, Nikiforidis G, Savva A, Giugni A, Wustoni S, Palanisamy T, Chen X, Maria IP, Di Fabrizio E, Costa PMFJ, McCulloch I, Inal S (2020) Biofuel powered glucose detection in bodily fluids with an n-type conjugated polymer. Nat Mater 19:456–463. https://doi.org/10.1038/s41563-019-0556-4
25. Paterson AF, Savva A, Wustoni S, Tsetseris L, Paulsen BD, Faber H, Emwas AH, Chen X, Nikiforidis G, Hidalgo TC, Moser M, Maria IP, Rivnay J, McCulloch I, Anthopoulos TD, Inal S (2020) Water stable molecular n-doping produces organic electrochemical transistors with high transconductance and record stability. Nat Commun 11:1–11. https://doi.org/10.1038/s41467-020-16648-0
26. Wang G, He X, Wang L, Gu A, Huang Y, Fang B, Geng B, Zhang X (2013) Non-enzymatic electrochemical sensing of glucose. Microchim Acta 180:161–186. https://doi.org/10.1007/s00604-012-0923-1
27. Li F, Liu Y, Shi X, Li H, Wang C, Zhang Q, Ma R, Liang J (2020) Printable and stretchable temperature-strain dual-sensing nanocomposite with high sensitivity and perfect stimulus discriminability. Nano Lett 20:6176–6184. https://doi.org/10.1021/acs.nanolett.0c02519
28. Ghaemmaghami M, Yamini Y, Mousavi KZ (2020) Accordion-like Ti3C2Tx MXene nanosheets as a high-performance solid phase microextraction adsorbent for determination of polycyclic aromatic hydrocarbons using GC-MS. Microchim Acta 187:1–8. https://doi.org/10.1007/s00604-020-4123-0
29. Shi YE, Han F, Xie L, Zhang C, Li T, Wang H, Lai WF, Luo S, Wei W, Wang Z, Huang Y (2020) A MXene of type Ti3C2Tx functionalized with copper nanoclusters for the fluorometric determination of glutathione. Microchim Acta 187:1–9. https://doi.org/10.1007/s00604-019-4000-x
30. Zhang J, Seyedin S, Qin S, Wang Z, Moradi S, Yang F, Lynch PA, Yang W, Liu J, Wang X, Razal JM (2019) Highly conductive Ti(3) C(2) T(x) MXene hybrid fibers for flexible and elastic fiber-shaped supercapacitors. Small. 15:e1804732. https://doi.org/10.1002/smll.201804732
31. Liu R, Miao M, Li Y, Zhang J, Cao S, Feng X (2018) Ultrathin biomimetic polymeric Ti(3)C(2)T (x) MXene composite films for electromagnetic interference shielding. ACS Appl Mater Interfaces 10:44787–44795. https://doi.org/10.1021/acsami.8b18347
32. Wang F, Yang C, Duan M, Tang Y, Zhu J (2015) TiO2 nanoparticle modified organ-like Ti3C2 MXene nanocomposite encapsulating hemoglobin for a mediator-free biosensor with excellent performances. Biosens Bioelectron 74:1022–1028. https://doi.org/10.1016/j.bios.2015.08.004
33. Li Q, Zhong B, Zhang W, Jia Z, Jia D, Qin S, Wang J, Razal JM, Wang X (2019) Ti(3)C(2) MXene as a new nanofiller for robust and conductive elastomer composites. Nanoscale. 11:14712–14719. https://doi.org/10.1039/c9nr03661j
34. Serafín V, Valverde A, Garranzo-Asensio M, Barderas R, Campuzano S, Yáñez-Sedeño P, Pingarrón JM (2019) Simultaneous amperometric immunosensing of the metastasis-related biomarkers IL-13Rα2 and CDH-17 by using grafted screen-printed electrodes and a composite prepared from quantum dots and carbon nanotubes for signal amplification. Microchim Acta 186. https://doi.org/10.1007/s00604-019-3531-5
35. Hurot C, Brenet S, Buhot A, Barou E, Belloir C, Briand L, Hou Y (2019) Highly sensitive olfactory biosensors for the detection of volatile organic compounds by surface plasmon resonance imaging. Biosens Bioelectron 123:230–236. https://doi.org/10.1016/j.bios.2018.08.072
36. Swynnerton NF, Huelle BK, Mangold DJ, Ludden TM (1986) A method for the combined measurement of ethiofos and WR-1065 in plasma: application to pharmacokinetic experiments with ethiofos and its metabolites. Int J Radiat Oncol Biol Phys 12:1495–1499. https://doi.org/10.1016/0360-3016(86)90202-6
37. Nishitani S, Sakata T (2020) Enhancement of signal-to-noise ratio for serotonin detection with well-designed nanofilter-coated potentiometric electrochemical biosensor. ACS Appl Mater Interfaces 12:14761–14769. https://doi.org/10.1021/acsami.9b19309

38. Ahmad K, Mohammad A, Mathur P, Mobin SM (2016) Preparation of SrTiO3 perovskite decorated rGO and electrochemical detection of nitroaromatics. Electrochim Acta 215:435–446
39. Li Z, Yin J, Gao C, Qiu G, Meng A, Li Q (2019) The construction of electrochemical aptasensor based on coral-like poly-aniline and Au nano-particles for the sensitive detection of prostate specific antigen. Sensors Actuators B295:93–100